Numerical Methods in Civil Engineering

K.N.T.U.

Numerical modeling of links behavior in eccentric bracings with dual vertical links

Saeid Sabouri-Ghomi* Behnam Saadati **

ARTICLE INFO

Article history:
Received:
October 2013.
Revised:
February 2014.
Accepted:
June 2014.

Keywords: Numerical Modeling, EBF-DVL, Vertical Link, Eccentrically Braced Frames, Hybrid Box Section

Abstract:

Configuration and geometry of bracing systems affect the seismic performance of structures significantly. Recently, the current authors have introduced a new configuration for eccentric bracing of structural frames that may be assumed as the combination of inverted Y-type and rotated K-type EBFs. The resulted braced frame is called EBF-DVL, consisting of two vertical links attached together by a horizontal link. For evaluating the vertical links of EBF-DVL in seismic conditions, a total number of 4 cyclic quasi-static tests were performed on the specimens with different link lengths, sections and material grades.

In this research, a summary of tests performed on experimental specimens are presented at first. Afterwards, the results of numerical modeling using ABAQUS software are described and compared with the experimental results. Cyclic loading was applied on each model, similar to the deformation history which was used during the tests. The effects of both material and geometry nonlinearities are considered. The diagrams of Load-displacement resulted from numerical analyses have a good agreement with the experimental ones; although there is more inconsistency in cases with steeper softening behavior. Also, the behavior of the links' components and yielding sequences are the same as experimental specimens.

1. Introduction

One of the most effective parameters in seismic behavior of a structural frame is employment of a proper bracing system. In recent years, some types of eccentrically braced frames are known as efficient seismic load resisting systems satisfying the stiffness and ductility requirements in relevant building code provisions. The investigators have mostly concentrated on EBFs with horizontal link beam (Roeder and Popov[11]; Hjelmstad and Popov[5]; Malley and Popov[7]; Kasai and Popov[6]; Engeldardt and Popov[2]). However, the preliminary tests were conducted on vertical link EBFs (Hisatoku et al[4]).

Some improper aspects of inverted Y-shape EBFs, such as low stiffness and possibility of out of plane buckling, are made them less efficient comparing with horizontal link EBFs.

However, considering the executive facilities, application of eccentric bracing with vertical links was developed recently in rehabilitation of concrete frames (Mazzolani[9]; Perera et al.[10]). EBFs with horizontal shear links have adequate stiffness and high ductility. However, as the link is typically a part of the floor beam, the replacement procedure after a design–level earthquake will be difficult and costly. On the other hand, this issue makes the design an iterative and exacting process, often resulting in oversized link elements, which leads to higher force demands in the other members of the EBF, including braces, columns, floor diaphragms, connections and foundations (AISC-341, 2010). In order to overcome this

* *Professor, Civil Engineering Department, K.N. Toosi University of Technology, Tehran Iran. Email : sabouri@kntu.ac.ir,*
***Corresponding Author: PhD, Civil Engineering Department, K.N. Toosi University of Technology, Tehran, Iran. Email : behnamsaadati@dena.kntu.ac.ir*

problem, some researchers focused on replaceable link beams (Fortney et al.[3]; Mansour et al.[8]). A common fact about the design of links implies the application of short links with shear yielding, which imposes small or no opening.

Recently, a new configuration for eccentric braces has been introduced by the current authors, which has two vertical links as energy dissipater components, hereafter called Eccentrically Braced Frame with Dual Vertical Links (EBF-DVL). The proposed bracing system improves some defects of conventional eccentric braces, having its own deficiencies. Here, it is not interested to describe the characteristics of proposed bracing system comprehensively; however, for integrity, the characteristics of the system are briefly presented.

EBF-DVL can be assumed as a combination of inverted Y-type (EBF with one vertical link) and rotated K-type (EBF with horizontal link between two braces) EBFs. It has two parallel vertical links which are connected to a horizontal link at the bottom and to the floor beam at the top. A schematic view of an EBF-DVL is demonstrated in Fig. 1. The upper mid region of EBF-DVLs, determined in the figure with dashed oval, is termed the "upper core".

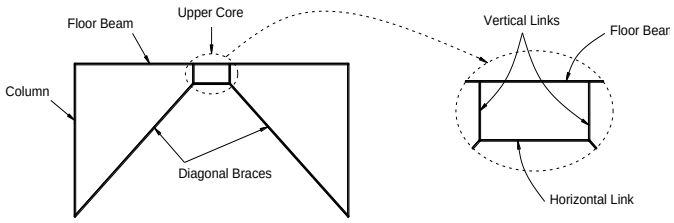

Fig.1: Schematic view of an EBF-DVL

EBF-DVL shall be designed in such a way that the deformation and yielding actions due to the lateral loads are occurred primarily within the vertical links. Capacity design principles should be considered in the design procedure of EBF-DVLs, similar to conventional EBFs. Hence, other members including horizontal links, floor beams, columns and diagonal braces essentially remain elastic under the maximum forces generated by the fully yielded and strain-hardened vertical links. Hereupon, all the main elements, including floor beam will experience no damage after a design-level earthquake. Hence, rehabilitation of the frame is readily executed by replacement of vertical links.

The authors conducted cyclic quasi-static tests on four specimens with different lengths and sections to evaluate the behavior of vertical links in EBF-DVLs. The main objective of the current research is proficiency of numerical method in the modeling of proposed bracing system by evaluating the behavior of vertical links. Therefore, conducted tests and obtained results are briefly described. Then, the summary and details of numerical simulation are presented. The numerical results are compared with those of experimental. ABAQUS software package was used to perform the numerical modeling.

2. Details of Specimens and Experimental Setup

The experimental setup as well as the typical dimensions is depicted in Fig. 2. Either of the 4 tested specimens consists of a lower horizontal deep beam, an upper horizontal beam and two built-up tubular vertical links welded to the beams at the top and bottom (similar to the upper core of EBF-DVL). The top and bottom beams were similar in all specimens and designed in such a way to remain in the elastic range with small deformations. The lengths of vertical links (e_H) are various in different specimens, leading to the specimens with different heights. However, the edge to edge distance of links was fixed at 600 mm.

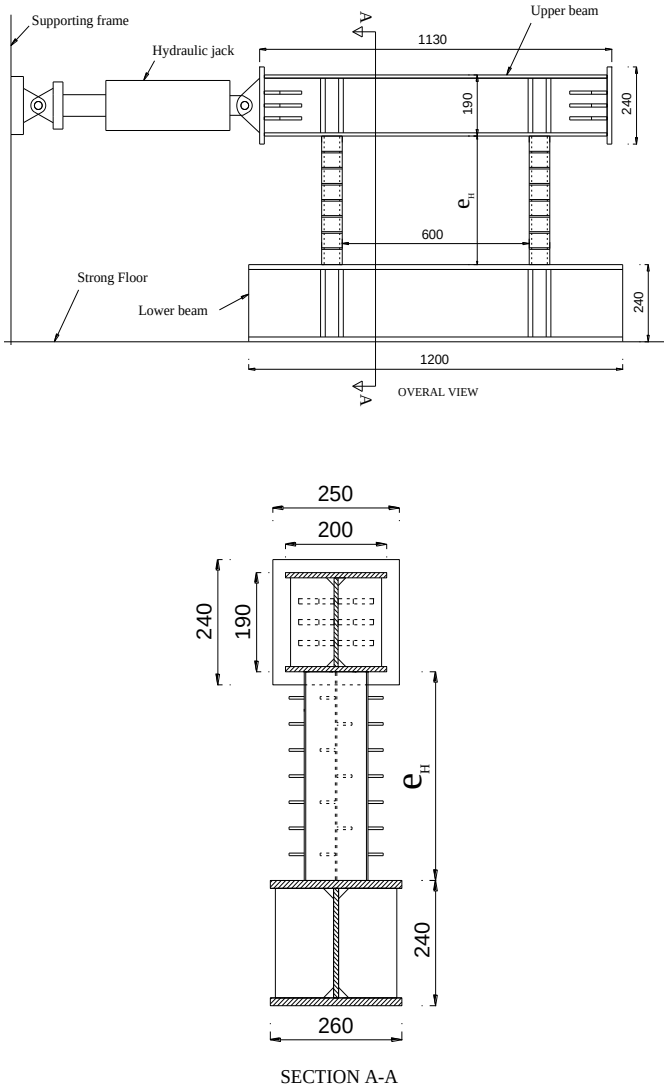

Fig.2: Experimental setup in each specimen

Cyclic horizontal excitation was statically imposed at one end of the top beam, while the lower flange of the bottom beam was bolted to the laboratory strong floor. Both jack connections, either to the specimen or to the supporting frame, were pinned to prevent any moment from being imposed on the specimen.

All links had hollow rectangular (tubular) cross sections, single closed box (section with two webs) or double connected closed boxes (section with three webs). Fig. 3 shows schematic configuration of a link with three webs. Since both links were similar in each specimen, only one of the links is shown in the figure. The vertical links of specimens were different in several parameters, such as material grade, link length, and shape and dimensions of cross section. The geometric parameters of the links are presented in Table 1.

It is known that the shear links behave much more ductile than bending links. Therefore, the specimens 1, 2 and 3 were designed as shear links and the specimen 4 as bending link. According to the AISC seismic provisions (AISC-341[1]), the links shorter than $1.6M_p/V_p$ are shear links, while the length of bending links are longer than $2.6M_p/V_p$.

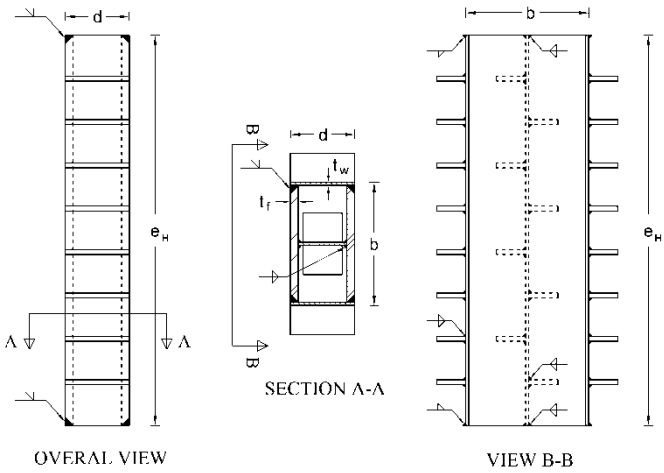

Fig. 3: The configuratuin of a vertical link section (with 3 webs)

Table 1. Dimensions of links

Specimen	b (mm)	d (mm)	t_f (mm)	t_w (mm)	N_w (Number	e_H (mm)
1	126	66	8	3	3	400
2	106	91	8	3	2	500
3	140	66	8	5	2	300
4	120	66	8	5	3	500

The material properties of steel plates obtained from tension coupon tests are tabulated in Table 2.

Table 2. Mechanical properties of steel plates

Plate Thickness (mm)	Modulus of Elasticity (MPa)	Yield Stress (MPa)	Ultimate Stress (MPa)	Elongation (%)
3	200000	182	269	41
5	200000	276	393	37
8	200000	315	437	32

3. Modeling

As mentioned before, ABAQUS software package was used for numerical modeling of the specimens. The top and bottom beams as well as the vertical links were meshed using S4 type shell elements. The mentioned element has 4 nodes with 6 degrees of freedom (3 translational and 3 rotational) in each node. The results are more precise using the structured meshing algorithm having the elements with approximate aspect ratios of one in the high stress intensity regions. Larger aspect ratios were used in the regions with predicted elastic behavior, such as top and bottom beams far from the vertical links. Fig. 4 illustrates the mesh pattern of the specimen 2.

The bolts between bottom beam of each specimen and strong floor of the laboratory constrained only translational movements. Therefore, in the numerical models, three displacement degrees of freedom were constrained in the corresponding nodes without constraining the rotational degrees of freedom. In order to observe the probable softening in load-displacement diagrams, the load was exerted as an increasing displacement on some nodes located at the middle height of the top beam. Static analyses were performed by considering the effect of large deformations. In order not to meet any inaccurate result, no energy dissipation methods were used to converge the results.

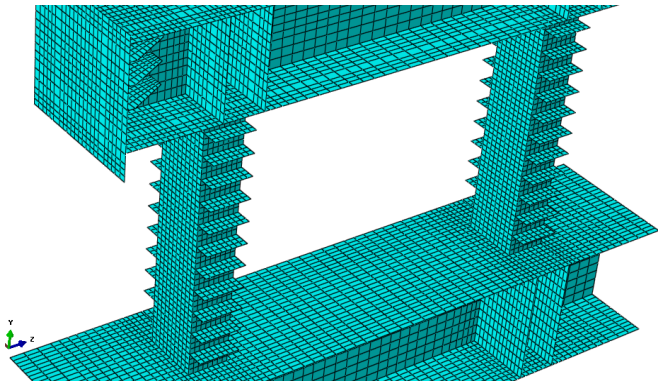

Fig. 4: Meshing pattern of the model corresponding to specimen 2

The plasticity model with combined hardening was preferred to the isotropic hardening, as strain reversal may occur in some regions of the model. In combined hardening plasticity model, both isotropic and kinematic hardenings can be regarded. Because of the diversity of required parameters for calibrating this model and the complexity of required tests, the isotropic term of hardening is neglected and just its kinematic term is considered. This model uses the Von Mises yielding surface and associated flow rule leading to formation of a symmetric stiffness matrix. ABAQUS considers the hardening region of this model as an exponential equation. Fig. 5 illustrates the schematic stress-strain curve of the applied model.

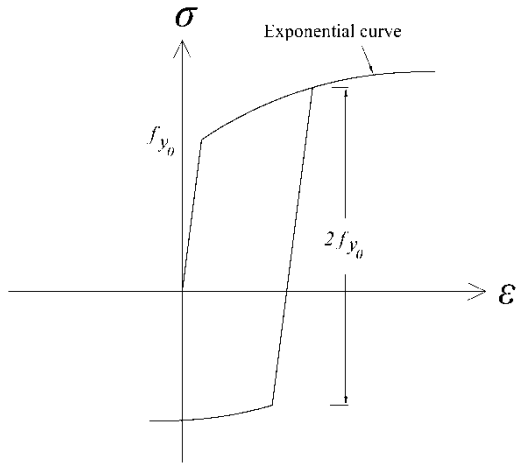

Fig. 5: Typical Stress-strain curve applied for combined hardening

As it can be seen, the bauschinger effect is assumed during the strain reversal. The hardening region of the stress-strain diagram (exponential curve) was calibrated using the stress-strain diagrams of the plates obtained from coupon tests.

4. Numerical Results

At the first, the overall results of numerical models are compared with those of experimental tests by using load-displacement diagrams. Concerning the links, it is customary to assess the results by load-rotation angle diagram, instead of load-displacement diagram. Both Links of each specimen have the same rotation angles (γ) which can be obtained from the following equation:

$$\gamma = \delta / e_H \quad (1)$$

where, γ is the rotation angle of the link; δ is the horizontal displacement at the middle height of the top beam; and e_H is the length of the link. Fig. 6 compares the numerical load-rotation angle diagrams with experimental ones. It should be noted that the experimental excitation was in the form of quasi-static cyclic loading, while the numerical models are made using monotonic loading. In the other word, the numerical load-rotation angle diagram is compared with the push of experimental hysteresis curve. Since the low-cycle fatigue resulted from the repeated loading cycles cannot be considered by the customary plasticity models for steel, therefore no remarkable difference is seen between the results of monotonic and cyclic loadings.

It could be observed that the numerical diagrams are in a good agreement with the experimental results, especially before the softening regime. The fracture occurred in the flanges of the box section links and also the separation of webs from the flanges along the welding line, led to the softening behavior during the experiments. Since the rules of continuum media were applied in numerical modeling, the mentioned fractures and separations were not considered in the models. Therefore, the strain softening regions have more differences in experimental and numerical results. In the event that the softening regime occurs due to reaching the steel to its ultimate limit, the differences would be reduced.

The experimental failures of specimens 1, 2 and 4 were because of the fractures at the top and bottom of the vertical links flanges at the connection to the top and bottom beams. The failure of specimen 3 occurred earlier than others and was due to the weld fracture along the web to flange connection line. The difference between fracture types led to rapid load degradation in specimen 3. Hence, as can be seen in Fig. 6, the difference between experimental and numerical results of this specimen is higher than those of three others. Yield and ultimate loads are presented in Table 3 for different specimens. The table indicates that the maximum difference between the experimental and numerical yielding loads is 8.5% and occurs in the specimen 3. This slight difference stands for the adequate ability of numerical modeling in estimating the yielding load of links. However, the difference increases for ultimate load, as its maximum in specimen 3 reaches to 27.7%.

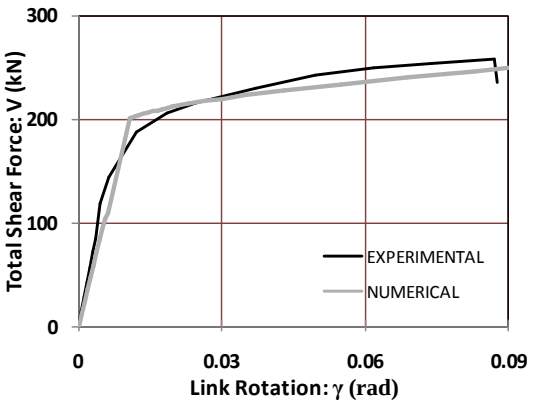

Specimen1

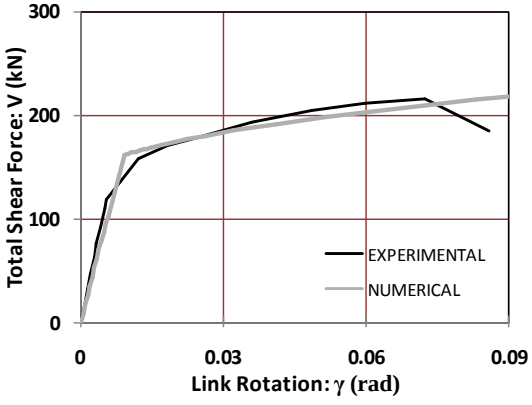

Specimen 2

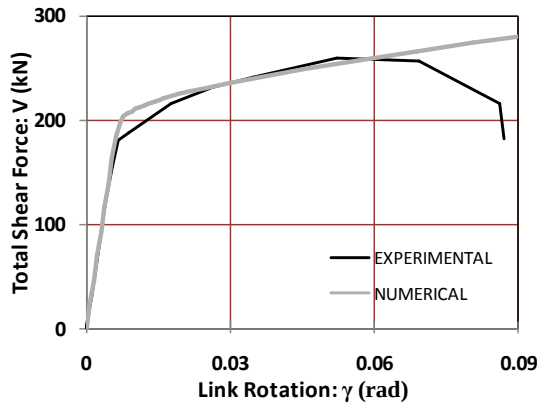

Specimen 3

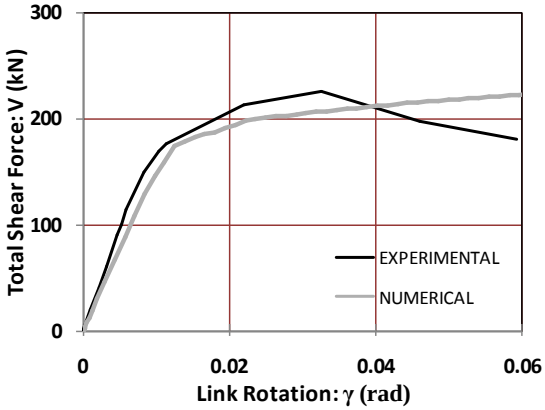

Specimen 4

Fig. 6: Typical Stress-strain curve applied for combined hardening

Table 3. Values of yielding and ultimate loads

Specimen	Yielding Load (kN)			Ultimate Load (kN)		
	Exp	Num	Diff (%)	Exp	Num	Diff (%)
1	188	201	6.9	236	250	5.9
2	158	161	1.9	185	216	16.7
3	187	203	8.5	216	276	27.7
4	176	174	1.1	180	222	23.3

The deformed shape of the models and also their Von Mises stress and equivalent strain counters will be investigated for more detailed assessment. Therefore, the deformed shapes of specimen 2 (with shear links) and also its corresponding model are demonstrated in Fig. 7. It can be seen that the deformation of the model is similar to that of the experimental specimen. Besides, similar to the results of the tests, no buckling is observed within the webs of the links. Hence, it can be stated that the deformed shape of this model is generally similar to the experimental deformation; this is also true for other specimens.

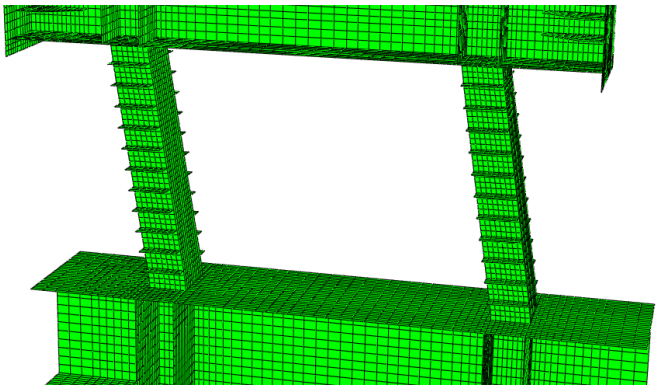

(a)

(b)

Fig. 7: The deformed shape of specimen 2: a) Model b) Experimental specimen

The contours of Von Mises and equivalent plastic strain are two main outputs for the steel material, as steel plasticity models mostly apply Von Mises yielding surface and the contour of equivalent plastic strain can demonstrate the yielding progression. These contours are depicted in Figs. 8 and 9 at two different moments (initial yielding occurrence and end of loading) in specimen 2 for the link near the loading point. From the equivalent plastic strain contour in Fig. 8, it could be deduced that the first yielding is initiated in the limited regions at the top and bottom of the webs, and not in the flanges. The yielding is gradually propagated in the whole regions of the webs and also at the top and bottom of the flanges (Fig. 9). This type of initiation and variation in plastic strain indicates the shear performance of the links. The experimental specimen is also demonstrated in Fig. 9 at a cycle near the end of the test (after considerable yielding, before the tearing of flanges and webs). The white wash splashing at the whole of the webs and at the top and bottom of the flanges shows the yielding regions and verifies the yielding regions obtained in the numerical model. A similar trend is observed in all three first specimens.

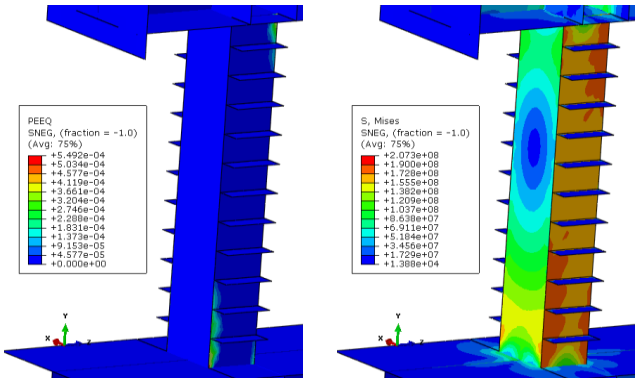

(a) (b)

Fig. 8: The contours of model 2 at the stage of initial yielding: a) Equivalent plastic strain; b) Von Mises stress

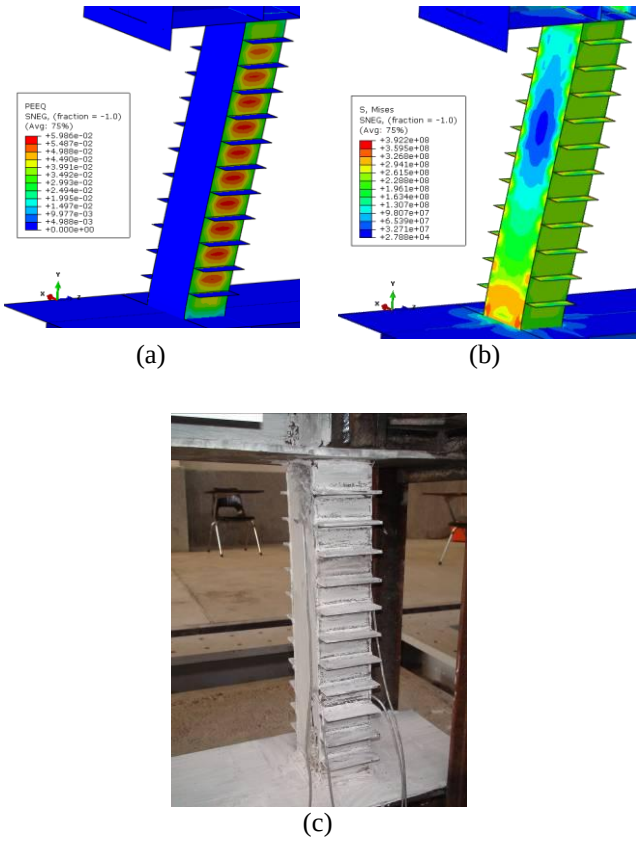

(a) (b)

(c)

Fig. 9: The model and specimen 2 at the end of loading: a) Equivalent plastic strain; b) Von Mises stress c) White wash splashing in the specimen

In the model corresponding to the specimen 4, unlike the three first models, the yielding is initiated at the top and bottom of the links' flanges. This is the behavior exactly expected in a bending link. The similar yielding regions were observed during the test, as the white wash on the top and bottom of the links' flanges initiate to splash earlier than the other parts of the links. In the numerical model, slight yielding points are also formed in the webs. Fig. 10 demonstrates the contours of equivalent plastic strain and Von Mises stress at the initial yielding moment. In addition, Fig. 10 shows splashing of white wash at the bottom of link's flange for the first yielding occurred in the laboratory.

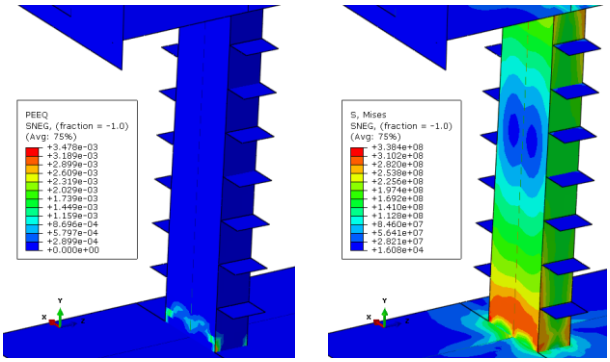

(a) (b)

(c)

Fig. 10: The model and specimen 4 at the initial yielding: a) Equivalent plastic strain; b) Von Mises stress c) White wash splashing in the specimen

In this model, the yielding extents at the top and bottom of the flanges and the amount of plastic strain increases as well. Slightly yielding also occurs at the top and bottom of the webs, without being propagated to the mid regions of the webs. Fig.11 illustrates the equivalent plastic strain and Von Mises stress in model 4. It clearly shows the bending behavior of the links. The yielding regions of the experimental specimen can also be seen in the figure. It continued until the fracturing of the flanges at the connections to the top and bottom beams.

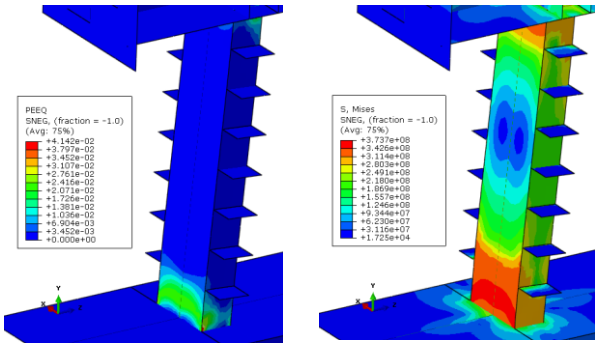

(a) (b)

(c)

Fig. 11: The model and specimen 4 at the end of loading: a) Equivalent plastic strain; b) Von Mises stress c) White wash splashing in the specimen

5. Conclusion

In this research, finite element method has been used to model 4 specimens from an experimental program performed on the upper core region of EBF-DVL. Numerical results were compared with the experimental outcomes, either in a view of overall behavior or in details. The following conclusions can be elicited from this research:

- The elastic and hardening regions of the load-rotation angle diagram for vertical links of EBF-DVLs can be properly predicted by finite element modeling.
- Softening behavior of vertical links was not observed in the numerical modeling. Therefore, the mentioned region of numerical load-rotation diagram was different from the experimental curve.
- Maximum difference between the numerical and experimental yielding loads was 8.5% related to the specimen 3. However, maximum ultimate load difference reached to about 27.7% in the specimen 3.
- In all models, the overall deformation pattern obtained from the numerical modeling was the same as experimental ones.
- There was a good agreement between the numerical and experimental results concerning the location of first yielding occurrence and its propagation. In shear links, initially, some limited regions in the webs of the links are yielded and then propagated to its other parts. However, in bending links, the yielding was initiated at the top and bottom of the links' flanges. In the continuation of loading, it increases around those regions and is propagated in the top and bottom of the webs.
- Generally, it seems that the behavior of vertical links in EBF-DVLs can be properly predicted by numerical modeling, concerning the load-rotation angle diagram or details of components behavior.

References

[1] AISC-341. 2010. Seismic Provisions for Structural Steel Buildings, Chicago.

[2] Engelhardt, MD., Popov, EP., 1989. On Design of Eccentrically Braced Frames. Earthquake Spectra: 5, 495-511.

[3] Fortney, PJ., Shahrooz, BM., Rassati, GA., 2007. Large-Scale Testing of a Replaceable "Fuse" Steel Coupling Beam. Journal of Structural Engineering, ASCE: 133, 1801-1807.

[4] Hisatoku, T., Segawa, T., Mukai, H., 1974. Experimental study on the static behaviour of the Y-typed bracings. Report No. 12, Takenaka Technichal Institute.

[5] Hjelmstad, KD., Popov, EP., 1983. Cyclic Behavior and Design of Link Beams. Journal of Structural Engineering, ASCE: 109, 2387-2403.

[6] Kasai, K., Popov, EP., 1983. General behavior of WF steel shear link beams. Journal of Structural Engineering, ASCE: 112, 362-382.

[7] Malley, J., Popov, EP., 1983. Design Considerations for Shear Links in Eccentrically Braced Frames. Report No. EERC 83-24. Earthquake Engineering Research Center, University of California, Berkeley, CA.

[8] Mansour, N., Christopoulos, C., Tremblay, R., 2011. Experimental Validation of Replaceable Shear Links for Eccentrically Braced Steel Frames. Journal of Structural Engineering, ASCE: 137, 1141-1152.

[9] Mazzolani, FM., 2008. Innovative metal systems for seismic upgrading of RC structures. Journal of Constructional Steel Research: 64, 882–895.

[10] Perera, R., Gómez, S., Alarcón, E., 2004. Experimental and Analytical Study of Masonry Infill Reinforced Concrete Frames Retrofitted with Steel Braces. Journal of Structural Engineering, ASCE: 130, 2032-2039.

[11] Roeder, CW., Popov, EP., 1977. Inelastic Behavior of Eccentrically Braced Steel Frames Under Cyclic Loadings. Report No. EERC 77-18. Earthquake Engineering Research Center, University of California, Berkeley, CA.